Plume Fluxes in Clear and Cloudy Convective Boundary Layers

Ulrich Schumann
DLR, Institute of Atmospheric Physics, D-8031 Oberpfaffenhofen
Federal Republic of Germany

and

Chin-Hoh Moeng
National Center for Atmospheric Research
P. O. Box 3000, Boulder, CO 80307

May 1990

submitted to the J. Atmos. Sci.

Abstract

From results of large-eddy simulations of the clear convective boundary layer (CBL) and of the stratus cloud-topped boundary layer (CTBL) we determine mean properties of "plumes" which consist of "updrafts" and "downdrafts." The plumes are defined locally by positive (for updrafts) or negative (for downdrafts) vertical velocity or by positive total moisture fluctuation or by a combination of both. The first two variants divide the motion field into two streams whereas in the third variant "environmental" air forms a separate stream. The results are in general agreement with existing measurements. From the results we compute mean vertical fluxes assuming "top-hat profiles" and compare these with the actual fluxes. Based on the qualitative agreement between these fluxes it is shown that the plume structure is best classified in terms of vertical velocity w. For such "w-plumes," the top-hat profile underestimates the actual fluxes by about a factor of 0.6.

1. Introduction

The motion in clear or stratus-cloud topped convective boundary layers exhibits a coherent structure of convective circulations composed of "updrafts" and "downdrafts," possibly separated by "environmental air." The updrafts are composed of quasi-steady large-scale plumes, which extent from the warm surface far up into the boundary layer, together with transient rising thermals which grow in size by lateral entrainment (Schmidt and Schumann, 1989; Moeng and Schumann, 1990). These structures carry a large portion of the vertical fluxes within the boundary layer and, hence, justify the "top-hat approximation" in which vertical fluxes $\overline{w'f'}$ are computed as if the vertical velocity w and the transported quantity f at a given height were constant within the two or three regions of motion. Let α_p denote the area fraction taken by updrafts ($p = u$), downdrafts ($p = d$), and environment ($p = e$), at a given height and let w_p and f_p denote the corresponding mean values of w and f, respectively. Then, previously proposed approximations (e.g. Betts, 1973, Greenhut and Khalsa, 1987, Manton, 1975, Businger and Oncley, 1990) are

$$\overline{w'f'} = \omega^{*}(f_u - \bar{f}), \quad \text{where } \bar{f} = \alpha_u f_u + \alpha_d f_d + \alpha_e f_e, \tag{1}$$

$$\overline{w'f'} = \omega^{**}(f_u - f_d), \tag{2}$$

$$\overline{w'f'} = a(\alpha_u w_u f_u + \alpha_d w_d f_d + \alpha_e w_e f_e), \tag{3}$$

$$\overline{w'f'} = b\sigma_w(f_u - f_d). \tag{4}$$

Here, ω^{*} and ω^{**} are "flux velocities," a and b are coefficients of order unity, and σ_w is the rms vertical velocity fluctuation. These approximations are applicable if a and b are about constant for all relevant quantities f, and if ω^{*} and ω^{**} are universal properties of convection, both for clear and cloudy cases. The parameter values depend on the criterion used to discriminate between the two or three regions of motion. In previous studies, the top-hat approximation was applied to scalar fluxes. Its applicability for fluxes of horizontal momentum ($f = u$) or vertical velocity variance ($f = w$) has not been tested.

Several experimental studies have considered the mean properties of plumes including the related fluxes. A wide variety of plume definitions has been used in the literature. Lenschow and Stephens (1980), for example, studied the convective boundary layer over the ocean and discriminated "thermals" from environmental air by requiring that the humidity be larger than a certain threshold for a sufficiently large distance within the thermal. Penc and Albrecht (1987) followed Nicholls and LeMone (1980) to investigate solid and broken cloud-topped mixed layers. They define updrafts as that part of a measured time-series having collocated positive values of vertical velocity and humidity fluctuations. Segments of the time-series where both quantities are negative are classified as downdrafts, leaving a remainder of environmental air which belongs to neither of these two classes. Greenhut and Khalsa (1987) identify an updraft (downdraft) in the marine atmospheric boundary layer when the vertical velocity fluctuation is larger (smaller) than a certain threshold value for a minimum time along the flight path of the measuring aircraft. Otherwise they classify the motion as belonging to environmental air. Young (1988) analyzed data from a convective boundary layer over land and defined updrafts and downdrafts in terms of either positive or negative spatially filtered vertical velocity. The filter excludes scales smaller than about one tenth of the boundary layer thickness. Further studies have been reviewed in the references just mentioned. Hence, practically every study is based on a different definition of plumes and thus conclusive comparisons cannot be made between the various studies. Moreover, the measurements apply to either clear or cloudy boundary layers and it is not obvious how the findings depend on the type of boundary layer.

In this paper we present analysis of large-eddy simulation results applying various types of plume definitions in order to find out for which classification the top-hat profile approximation gives the most consistent results for various conserved quantities. Moreover, we present results from two types of boundary layers (the CBL and the CTBL, details are given in the next chapter) to get at least some indication on how far various characteristics of plumes are affected by the type of flow.

Large-eddy simulations (LES, see the review by Nieuwstadt, 1990) resolve the energy carrying eddies while modelling subgrid-scale (SGS) contrib-

utions. Such simulations with fine resolution have been shown to be very successful in simulating the characteristic features of buoyancy dominated clear boundary layers, because the large-scale flow structures, such as plumes or thermals can be accurately resolved. Relatively few simulations have been performed for cloud-topped boundary layers (Deardorff, 1980, Moeng, 1986, 1987).

For the present study, we use the results from the LES-code of Moeng (1984, 1986). We apply the LES results just as experimental data and assess their validity by comparing to experimental results where possible and by comparing the magnitude of the observed effects relative to SGS-contributions. The conditional averaging procedure will be based solely on the resolved field. Thus our approach is similar to experimental studies which use filtered fields to classify the plume type or which require the indicator function to persist over a certain interval.

2. The large-eddy simulation data

The method for the clear convective boundary layer CBL and the parameters of the simulations, employing 96^3 grid points, are as described in Moeng (1984), and Moeng and Wyngaard (1989). The (equidistant) grid spacings are $\Delta x = \Delta y = 52.083$ m in the horizontal directions and $\Delta z = 20.833$ m in the vertical. The results for the CBL are scaled using the convective velocity scale w_* and the temperature scale T_* which are based on the surface heat flux, the height of the boundary layer z_i (actually the height where the vertical heat flux takes its minimum value) and the buoyancy parameters. The ratio between boundary layer height z_i and Obukhov-length L amounts to -14 (friction velocity $u_* = 0.589$ ms^{-1}, $w_* = 2.02$ ms^{-1}, $z_i = 1030$ m).

Figure 1 depicts various normalized mean profiles of the CBL. We observe the well mixed part of the CBL with close to uniform potential temperature below the inversion. The strong mixing in this layer is also reflected in the velocity profiles. Rather strong shear appears at the inversion and near the surface. Shear and buoyancy drive the turbulent motion with resultant velocity variance as shown in Fig. 1c. In the mixed layer, the variance is

largest for vertical velocity which indicates strong updrafts and downdrafts. The lateral motion from downdrafts to updrafts near the surface is responsible for the large variances in the horizontal velocity components near the surface and similar near the inversion. The fact that the variance of v' is larger than that for u' indicates that part of the turbulent motions is organized in the form of rolls with axis in the downstream direction. The kinetic energy e in the subgrid scales is small (less than 15 %) in comparison to the energy E of all scales. Figure 1a also shows the energy dissipation; other components of the kinetic energy budget have been reported by Moeng and Wyngaard (1989). In this case, shear contributes only little to energy production except near the surface. Turbulence transports energy upwards towards the inversion where buoyancy production is negative and enhances the energy destruction by dissipation.

The method for the cloudy case (CTBL) and the parameters are as described in Moeng (1986), simulation case I, except that the code was rerun with 80^3 grid points instead of 40^3. The vertical grid width has been halfed to 12.5 m. The horizontal grid spacing (62.5 m) is the same as in Moeng (1986) but the size of the computational domain has been doubled horizontally to cover 5 km x 5 km x 1 km. The larger horizontal domain size allows for the formation of larger scales and reduces statistical uncertainty in approximating ensemble means by horizontal mean values. The surface is kept at constant temperature and saturated moisture. The results are normalized by a convective velocity w_* which is based on the averaged total buoyancy flux inside the cloud layer (Moeng, 1986) or by the velocity scale $w_{*D} = [2.5\, T^{-1} g \int_0^{z_i} \overline{w'\theta'_v} dz]^{1/3}$ introduced by Deardorff (1980). On average, $w_* = 0.829$ ms^{-1}, $w_{*D} = 1.102$ ms^{-1}, $u_* = 0.300$ ms^{-1}, $z_i/L = -20$.

Mean profiles, see Fig. 2, compare closely to previous results (Moeng, 1986, 1987). The boundary layer possesses a strong inversion near $z_i = 507$m below which a 312 m thick solid layer of stratus cloud forms. The liquid water content grows with height in close agreement with adiabatic mixing. The wind profile is similar to that in the dry case. The inversion extends over only 2 vertical grid cells. The case under consideration is driven by both longwave radiation cooling at the top and the surface buoyancy flux as reflected by the total heat flux profile in Fig. 2d and the buoyancy production term B, see Fig. 2e, which equals the flux of virtual potential tem-

perature. Shear (curve S in Fig. 2e) contributes significantly only near the surface and at the inversion. Turbulent transport (term D in Fig. 2e) again balances the energy loss by dissipation ($-\varepsilon$) and buoyancy at the inversion. The profiles of velocity variances and kinetic energy E, Fig. 2e, have a shape which is similar to that in the dry case except that cloud forcing has caused larger variances in the upper part of the boundary layer.

3. Conditional sampling method

We determine conditional mean values f_p of any quantity f for either of the three classes $p = u, d, e$ from averages over all discrete grid points, $i = 1,...,M_x$, $j = 1,...,M_y$ in a horizontal plane at height z,

$$f_p(z) = \sum_{i=1}^{M_x}\sum_{j=1}^{M_y} I_p(x_i, y_j, z)\, f(x_i, y_j, z) \Big/ \sum_{i=1}^{M_x}\sum_{j=1}^{M_y} I_p(x_i, y_j, z), \tag{5}$$

where I_p is the "indicator function" that discriminates between "updrafts" (I_u), "downdrafts" (I_d), and possibly "environmental air" (I_e) through the following definitions:

1) "w-plumes" using vertical velocity: $I_u(x,y,z,t) = 1$ if $w(x,y,z,t) > w_{th}^+$, $I_u = 0$ otherwise; $I_d(x,y,z,t) = 1$ if $w(x,y,z,t) \leq w_{th}^-$, $I_d = 0$ otherwise; $I_e = 1 - I_u - I_d$. In general and for comparison with Young (1988), we assume zero threshold values $w_{th}^+ = w_{th}^- = 0$, so that the set of grid points with environmental air is empty. However for comparison with the experimental results of Greenhut and Khalsa (1987) we apply their definitions where the threshold values equal half the variances of positive and negative vertical velocity fluctuations. In order to compare with Nicholls (1989), we set $w_{th}^+ = w_{th}^- = -0.5\, w_{*D}$.

2) "q-plumes" like w-plumes but using total moisture instead of vertical velocity and zero threshold values.

3) "wq-plumes" using vertical velocity combined with moisture: $I_u(x,y,z,t) = 1$ if $w(x,y,z,t) > 0$ and $q'(x,y,z,t) > 0$, $I_u = 0$ otherwise;

$I_d(x,y,z,t) = 1$ if $w(x,y,z,t) < 0$ and $q'(x,y,z,t) < 0$, $I_d = 0$ otherwise; $I_e = 1 - I_u - I_d$.

In the clear CBL we use potential temperature instead of moisture to obtain "T-plumes" or "wT-plumes." We cannot compare with Lenschow and Stephens (1980) because the LES of the clear CBL has been performed without moisture. Note that the classification is based on the resolved fields w, T and q. This is consistent with the usage of filtered measurements by experimentalists. Local values of the fluxes are computed as sums of grid mean values plus modelled subgrid-scale contributions. To reduce statistical errors, the results have been averaged over 8 (for CBL) or 6 (for CTBL) discrete time points from a time period of 1920 s (CBL) of 1000 s (CTBL) for which data are available.

4. Comparison with experiments

Several authors have reported conditional mean values based on measurements in clear or cloudy boundary layers to which we can compare. The results obtained from LES of the CBL are compared, e.g., in Fig. 3 with data of Young (1988). The measurements are taken in a cloud-free CBL over land. The analysis distinguishes between updrafts and downdrafts according to "w-plumes." The shapes of the computed and the measured profiles of the area fraction of updrafts and the corresponding updraft velocities agree closely with results obtained from other LES results (Schumann, 1989). The area fraction taken by updrafts is smaller than 0.5 in the mixed layer. As a consequence of continuity, the vertical velocity magnitude is larger in updrafts than in downdrafts. This is consistent with a positive skewness of the vertical velocity (Wyngaard, 1987, Moeng and Rotunno, 1990). Updrafts are warmer than downdrafts, as to be expected, in the mixed layer. The reduction in temperature difference very close to the surface is presumably caused by insufficent resolution of small-scale plumes in the LES at this level. At the inversion, updrafts are rising beyond buoyant equilibrium because of their inertia and this agrees qualitatively with the measurements. The quantitative differences between measured and computed values are small and this confirms the validity of the LES data. Based on results from Lenschow and Stephens (1980) and previous LES-data,

Chatfield and Brost (1987) proposed a model in which α_u decreases linearly from 0.655 at the bottom surface to 0.076 at the inversion and where the plume velocity profiles have much different shape. This result does not apply to w-plumes. The plume flux $\alpha_u w_u$ reaches $0.175 w_*$ in their model but about $0.23 w_*$ in the present results.

Figure 4 shows the LES-results for profiles of the mean diameters. of updrafts and downdrafts and the number N of updrafts per unit length. These parameters are computed as explained in the appendix. The computed maximum values of the mean diameters are little smaller than the maximum values reported by Young (1988) for the "width," i.e. $0.45\, z_i$ for updrafts and $0.55\, z_i$ for downdrafts. Young found that the number density of plumes ranged from 1.4 to 2.8 with no detectable vertical trend. These results are roughly consistent with our numerical results.

The results shown in Figs. 5 to 7 have been evaluated from the same LES data for w-plumes with the threshold definitions of Greenhut and Khalsa (1987). The threshold value profiles reach extreme values $w_{th}^- = -0.5\, w_*$ and $w_{th}^+ = 0.8\, w_*$ near $z/z_i = 0.4$. The measurements have been obtained in a maritime cloud-free CBL. Again, the agreement between measured and computed data is very good but the results are much different from Young's results and those reported by Lenschow and Stephens (1980) according to the different criterion used.

The results, Fig. 5, show that updrafts and downdrafts with large vertical velocity occupy only about 20 % of the total area. Their diameter increases from the surface up to the upper third of the mixed layer. The number of updrafts per unit length is smaller than the number of downdrafts. The updraft velocity, Fig. 6, is larger than the downdraft velocity and these values are larger in the criterium of Greenhut and Khalsa than in that of Young. Updrafts carry most of the momentum flux. This can be seen from the larger difference in horizontal velocity shown in Fig. 6 and in the larger flux values from updrafts shown in Fig. 7. Figure 7 shows also that most of the vertical heat flux is carried by the strong updrafts. The normalized profiles agree with those of Greenhut and Khalsa (1987) to a surprisingly large degree although details of the mean velocity profile and surface friction are different.

In Fig. 8, LES data are compared with data of Nicholls (1989) for a CTBL. The LES-data refer to downdrafts defined as w-plumes with $w_{th}^{-} = 0.5\, w_{*D}$. Nicholls defined segments of aircraft data of vertical velocity fluctuations between zero values as downdrafts which at least partly exceeded a downward velocity of $-0.5\, w_{*D}$. Such a non-local criterion is difficult to implement in the LES-analysis. As a consequence, Nicholls' method selects little weaker downdrafts than our analysis. Partly because of the difference in the sampling procedure, the agreement is less perfect for the CTBL than for the clear case. In particular, the measurements indicate that the downdrafts are of smaller diameter and larger frequency and occupy a larger area than in the simulations. This may be caused by a still too coarse horizontal resolution in the LES for this CTBL case; a diameter of $0.2\, z_i$ corresponds to only two horizontal grid cells. However, differences will also be caused by different buoyancy forcing. Nicholls' cases are driven by top-cooling with very little surface heating.

Figures 9 and 10 show results obtained from case CTBL for wq-plumes. Such plumes were considered before by Nicholls and LeMone (1980) and by Penc and Albrecht (1987). The latter authors report average area fractions of 0.28 to 0.29 for updrafts, 0.27 to 0.31 for downdrafts and 0.41 to 0.44 for environmental air from measurements for various cases. They do not report profiles for these quantities but our LES results show little variation with altitude. The computed results for the area fractions are close to the data reported by Penc and Albrecht (1987).

Figure 10 shows differences between updraft and downdraft moisture and temperature profiles. Updrafts have larger moisture than downdrafts because that is a condition entering the criterion of wq-plumes. In the lower part of the boundary layer this difference is caused by surface evaporation. The difference decreases with increasing height because of lateral mixing between updrafts and downdrafts. The moisture difference becomes very large at the inversion because downdrafts from above the inversion carry very dry air. The magnitude of this difference reflects the strong vertical decrease in the mean moisture profile at this level. Because of surface heating, the updrafts are warmer than downdrafts for most of the mixed layer by up to six units of the convective temperature scale T_{*D} in rough agreement with the results for the dry CBL, see Fig. 6b. In the stratus layer,

water condenses, resulting in positive differences in liquid water content between updrafts and downdrafts. This causes additional buoyancy forcing of the circulation as reflected by the differences in virtual potential temperature. But the updrafts are colder than downdrafts at the inversion because updrafts rise beyond the level of zero buoyancy (virtual temperature difference) into the much warmer air above the inversion. The data points are taken from Penc and Albrecht (1987). The absolute values differ considerably because of differences in the absolute values of the fluxes and the changes in mean temperature and moisture at the inversion. Therefore, the data have been normalized and plotted according to the upper ordinate in Fig. 10. Here we use the convective scales of temperature T_{*D} and moisture q_{*D} such that $w_{*D}T_{*D}$ equals the mean vertical temperature flux and $w_{*D}q_{*D}$ the mean vertical moisture flux averaged from $z = 0$ to $z = z_i$, where w_{*D} is Deardorff's velocity scale as defined in section 2. From the data of flights 4 and 5 analyzed by Penc and Albrecht (1987) we determine $w_{*D} =$ 0.54, 0.31 ms^{-1}, $T_{*D} =$ 0.007, 0.0023 K, $q_{*D} =$ 0.016, 0.011 g/kg, for the two flights, respectively. In the LES-results, the corresponding scales are $T_{*D} = 0.027$ K, $q_{*D} = 0.017$ g/kg. The normalized data agree quite well with the simulated results. In the subcloud layer, the results are of a magnitude which is roughly comparable with data reported by Nicholls and LeMone (1980) although details differ.

These results show that the simulations for the CTBL agree sufficiently with observations so that the parameters of Eqs. (1 - 4) can be determined.

5. Top-hat profile parameters

Horizontally averaged flux values versus height (full curves) for various transported quantities are shown in Fig. 11 for the CBL and in Fig. 12 for the CTBL. Also plotted are the contributions from plumes according to the simple top-hat approximation

$$\overline{w'f'} \approx (\alpha_u w_u f_u + \alpha_d w_d f_d + \alpha_e w_e f_e). \qquad (6)$$

The various curves apply to different types of plume definitions. In general, the top-hat approximation underestimates the actual flux profiles which means that the coefficient a in Eq. (3) should be larger than unity. The

strong reduction of the approximated fluxes in the lowest 10 % of the boundary layer is caused by insufficient resolution of the narrow plumes near the surface. Here, most of the total fluxes in the LES are carried by subgrid-scale motions.

From Fig. 11, for the CBL, we see that w-plumes give about the same contributions from top-hat profile approximations as do T-plumes with respect to the temperature flux but T-plumes underestimate plume contributions to the momentum flux and to vertical velocity variance. However, we see that the w-plume results are uniformly smaller than all the actual fluxes by a factor which is of the order 0.6 and close to constant throughout the mixed layer $0.1 \leq z/z_i \leq 0.8$. This is the first indication that w-plumes are more meaningful than other types of plume definitions.

Figure 12 shows similar comparisons for the CTBL, including fluxes of non-conserved quantities like buoyancy or liquid water. The top-hat approximations partly overestimate the actual flux magnitudes considerably, which would imply $a < 1$. Especially, the wq-plumes (short-dashed curves) give much too large moisture flux at the inversion. This is partly a consequence of the criterion which selects those plumes with large correlation between moisture and vertical velocity. The overestimate is particularly large at the inversion where dry air entrained from above the inversion exhibits large negative moisture fluctuations correlated with negative vertical velocity. The wq-plumes also overestimate the entrainment heat flux because entrained air exhibits negative moisture fluctuations but positive temperature deviations. The q-plumes (dash-dotted curves) result in flux profiles which differ qualitatively from the actual flux profiles not only at the inversion but also in the mixed layer. Obviously, only w-plumes (long-dashed curves) give meaningful top-hat approximations. This is not surprising because w-plumes are defined according to the vertical velocity which is reponsible for vertical turbulent transport.

In Fig. 13, we show results from evaluations of the coefficients a and b and the flux velocity ω^* defined in Eq. (1) using w-plumes. Profiles of ω^{**} are not plotted because, by definition, $\omega^{**}/\omega^* = \alpha_d \cong 0.5$ for plume definitions which distinguish between updrafts and downdrafts only. In this case, $\alpha_e = 0$, and continuity implies $\alpha_d\omega^* = \omega^{**} = a\alpha_u w_u = b\sigma_w$. The results are shown only for

$z > 0.1\, z_i$ because the LES underestimates plume contributions from small-scale motions near the surface. This underestimate causes a strong increase in the coefficients near the surface while Businger and Oncley (1990), from unfiltered data, find an almost constant value $b \cong 0.6$ even at very small altitudes. In Fig. 13, the flux velocities are normalized by w_{*D}. Penc and Albrecht (1987) proposed to normalize by $(\omega_{*D}^2 + 4u_*^2)^{1/2}$. However, this normalization gives only small differences because of the smallness of u_*/w_{*D} in the present simulations.

We find that the coefficients a and b are not strictly constant and not strictly independent of the transported quantity. The results show large fluctuations in the upper part of the mixed layer because both the fluxes and the plume differences get small or even change sign there but not exactly at the same altitude. Hence, the top-hat approximation is meaningful only in the mixed layer, i.e. for $z/z_i \lesssim 0.8$. Much larger variations have been found in comparable plots (not shown) for q-plumes (T-plumes) and wq-plumes (wT-plumes). The differences between the various curves are larger in the CTBL than in the CBL. This might originate from the more complicated physics of the CTBL compared to the CBL. The results for coefficient a at various heights and for various transported quantities f show less scatter than those for b. This reflects the more complete physical content of Eq. (3) in comparison to Eq. (4) which does not account for differences in the vertical velocities inside the plumes.

The largest degree of uniformity of the coefficients and flux velocities for the various transported quantities has been found for w-plumes with threshold values as defined by Greenhut and Khalsa (1987). Figure 14 shows, e.g., the LES-results for ω^{**} in w-plumes in comparison with experimental data for the CBL. The magnitude of ω^{**} is close to the values reported by Betts (1976) and Nicholls and LeMone (1980) who considered wq-plumes.

Further evaluations of the mixed layer of the CBL in w-plumes with such threshold values as used by Greenhut and Khalsa (1987) result in $a \cong 1.3 \pm 0.1$, $b \cong 0.3 \pm 0.05$, $\omega^*/w_* \cong 0.3 \pm 0.1$.

6. Conclusions

The LES results compare generally very well with observations. Obviously, the LES method has become a validated tool to predict properties of convective boundary layers. The differences for the CTBL are somewhat larger than for the CBL which indicates either effects of physical processes not covered by the model like solar radiation or the actual inversion properties or deficiencies due to insufficient grid resolution. The CBL-simulations cover both the properties of clear CBL over land and of the cloud-free CBL over sea. Hence, physical processes other than the surface heat and moisture fluxes are of little importance for convective boundary layers. The results match very well with the nowadays well established convective scales. Most consistent top-hat approximations are found in terms of w-plumes. For such w-plumes with zero threshold values, for the mixed layer of the CBL, we recommend $a \cong 1.6 \pm 0.1$, $b \cong 0.6 \pm 0.1$. Hence, the top-hat approximation describes $a^{-1} \cong 0.625 \pm 0.04$ or about 60 % of the total fluxes of all relevant quantities. The top-hat approximation gives a fair approximation not only for scalar fluxes but also for fluxes of horizontal momentum and for the vertical velocity variance. For the CTBL somewhat larger scatter is observed. The value of ω^*/w_{*D} is not so constant and of order 0.7. In a subsequent paper, we will consider budgets of various fields within plumes.

Acknowledgments. This work was started while the first author was on sabatical leave with the National Center for Atmospheric Research. The National Center for Atmospheric Research is sponsored by the National Science Foundation.

Appendix. Geometrical parameters of plumes

In this appendix some geometrical parameters of plumes are defined and it is shown how they are computed from the know indicator function I_p for a plume of type p. The indicator function is defined for each grid index i, j of the $M_x \cdot M_y$ grid cells in a horizontal plane at height z of the computational domain. The grid spacings in the three directions Δx, Δy, Δz are constants in our simulations. The computational domain covers the horizontal area $A = M_x M_y \Delta x \Delta y$. The horizontal cross-section taken by the plumes within the

computational domain at any height is $A_p = \Delta x \Delta y \sum_{i=1}^{M_x} \sum_{j=1}^{M_y} I_p(i, j)$. The fractional area of the plumes at heigth z equals $\alpha_p = A_p / \bar{A}$. The mean numbers of plumes per unit length z_i in x and y-directions are computed from

$$N_{xp} = \frac{z_i}{M_x \Delta x} \frac{1}{M_y} \sum_{j=1}^{M_y} \frac{1}{2} \sum_{i=1}^{M_x} |I_p(i+1, j) - I_p(i, j)|,$$

$$N_{yp} = \frac{z_i}{M_y \Delta y} \frac{1}{M_x} \sum_{i=1}^{M_x} \frac{1}{2} \sum_{j=1}^{M_y} |I_p(i, j+1) - I_p(i, j)|. \tag{7}$$

Here, the innermost sums count the number of intersections of a plume surface with a grid-line in the computational domain. The outer sums perform the average over all parallel lines and the remaining factors provide the proper normalization. The mean length taken by plumes along either of the two horizontal coordinate directions are

$$d_{xp} = \alpha_p z_i N_{xp}^{-1}, \quad d_{yp} = \alpha_p z_i N_{yp}^{-1}. \tag{8}$$

A mean diameter $\bar{d}_p$ of the plumes can be defined, following Lenschow and Stephens (1980), from an equivalent circular plume having the cross-section A_p and perimeter P_p of the actual plumes so that

$$\bar{d}_p = 4 A_p P_p^{-1}. \tag{9}$$

The perimeter P_p is evaluated from

$$P_p = \frac{\pi}{4} \frac{A}{z_i} 2 (N_{xp} + N_{yp}), \tag{10}$$

where the factor $\pi/4$ is included, again following Lenschow and Stephens (1980), to reduce the perimeter of the polygonal circumference to that of an equivalent circle. The mean diameter is related to the mean lengths by

$$\bar{d}_p^{-1} = \frac{\pi}{8} (d_{xp}^{-1} + d_{yp}^{-1}). \tag{11}$$

Where possible without ambiguity, the index p is omitted.

References

Betts, A. K., 1973: Non-precipitating cumulus convection and its parameterization. *Q. J. R. Meteor. Soc.*, **99**, 178-196.

Betts, A. K., 1976: Modeling subcloud layer structure and interaction with a shallow cumulus layer. *J. Atmos. Sci.*, **33**, 2363-2382.

Businger, J. A., and Oncley, S. P., 1990: Flux measurements with conditional sampling. J. Atmos. Ocean. Techn., to appear

Chatfield, R. B., and R. A. Brost, 1987: A two-stream model of the vertical transport of trace species in the convective boundary layer. *J. Geophys. Res.*, **92**, D11, 13263-13276.

Deardorff, J. W., 1980: Stratocumulus-capped mixed layers derived from a three-dimensional model. *Boundary-Layer Meteor.*, **18**, 495-527.

Greenhut, G. K., and S. J. S. Khalsa, 1987: Convective elements in the marine atmospheric boundary layer. Part I: Conditional sampling statistics. *J. Clim. Appl. Meteor.*, **26**, 813-822.

Lenschow, D. H., and P. L. Stephens, 1980: The role of thermals in the convective boundary layer. *Boundary-Layer Meteor.*, **19**, 509-532.

Manton, M. J., 1975: Penetrative convection due to a field of thermals. *J. Atmos. Sci..*, **32**, 2272-2277.

Moeng, C.-H., 1984: A large-eddy-simulation model for the study of planetary boundary-layer turbulence. *J. Atmos. Sci.*, **41**, 2052-2062.

Moeng, C.-H., 1986: Large-eddy simulation of a stratus-topped boundary layer. Part I: Structure and budgets. *J. Atmos. Sci.*, **43**, 2886-2900.

Moeng, C.-H., 1987: Large-eddy simulation of a stratus-topped boundary layer. Part II: Implications for mixed-layer modeling. *J. Atmos. Sci.*, **44**, 1605-1614.

Moeng, C.-H., and R. Rotunno, 1990: Vertical-velocity skewness in the buoyancy-driven boundary layer. *J. Atmos. Sci.*, **??**, in print.

Moeng, C.-H., and U. Schumann, 1990: Composite updraft and downdraft in stratus-topped boundary layer. Proc. 9th Symp. on Turbulence and Diffusion, April 29-May 3, Roskilde, Denmark, Americ. Met. Soc., pp. 7-10.

Moeng, C.-H., and J. C. Wyngaard, 1988: Spectral analysis of closures for pressure-scalar covariances in the convective boundary layer. *J. Atmos. Sci.*, **45**, 3573-3587.

Moeng, C.-H., and J. C. Wyngaard, 1989: Evaluation of turbulent transport and dissipation closures in second-order modeling. *J. Atmos. Sci.*, **46**, 2311-2330.

Nicholls, S., 1989: The structure of radiatively driven convection in stratocumulus. *Q. J. R. Meteorol. Soc.*, **115**, 487-511.

Nicholls, S., and M. A. LeMone, 1980: Fair weather boundary layer in GATE: The relationship of subcloud fluxes and structure to the distribution and enhancement of cumulus clouds. *J. Atmos. Sci.*, **37**, 2051-2067.

Nieuwstadt, F. T. M., 1990: Direct and large-eddy simulation of free convection. Proc. 9th Intern. Heat Transfer Conference, Jerusalem, 19-24 August 1990, pp. 25. Preprint available from Techn. Univ. Delft, Rotterdamseweg 145, 2628 AL Delft, the Netherlands.

Penc, R. S., and B. A. Albrecht, 1987: Parametric representation of heat and moisture fluxes in cloud-topped mixed layers. *Boundary-Layer Meteor.*, **38**, 225-248.

Schmidt, H., and U. Schumann, 1989: Coherent structure of the convective boundary layer derived from large-eddy simulations. *J. Fluid Mech.*, **200**, 511-562.

Schumann, U., 1989: Large-eddy simulation of turbulent diffusion with chemical reactions in the convective boundary layer. *Atmos. Environ.*, **23**, 1713-1727.

Wyngaard, J. C., 1987: A physical mechanism for the asymmetry in top-down and bottom-up diffusion. *J. Atmos. Sci.*, **44**, 1083-1087.

Young, G. S., 1988: Turbulence structure of the convective boundary layer. Part II: Phoenix 78 Aircraft observations of thermals and their environment. *J. Atmos. Sci.*, **45**, 727-735.

FIGURE LEGENDS

Fig. 1. Mean profiles in the CBL. (a) potential temperature and normalized dissipation rate, (b) horizontal wind components, (c) turbulent kinetic energy of all scales E, subgrid-scale kinetic energy e, and energy of the three velocity components.

Fig. 2. Mean profiles in the CTBL. (a) liquid water potential temperature (full curve) and virtual potential temperature (dashed), (b) total and liquid water content, (c) wind components, (d) sum of liquid water static energy and longwave radiation fluxes (full curve) and liquid water static energy flux alone (dashed), (e) budget of kinetic energy due to buoyancy B, shear S, dissipation ε, and diffusion D, (f) total kinetic turbulence energy E, SGS energy e, and variance components.

Fig. 3. Comparison of w-plume mean values computed from LES for case CBL (full curves) with measured data (symbols) and corresponding interpolations (dashed curves) from Young (1988). (a) Area fraction of updrafts, (b) updraft and downdraft velocities, (c) potential temperature deviations in updrafts and downdrafts relative to the horizontally averaged potential temperature.

Fig. 4. Mean diameters $\bar{d}$ of updrafts and downdrafts and number N of updrafts per unit length (averaged over both horizontal directions) for case CBL, w-plumes.

Fig. 5. Comparison of plume mean values computed for case CBL (curves without symbols) with measured data (curves with symbols) from Greenhut and Khalsa (1987). Full curves and Δ: updrafts, dashed curves and ∇: downdrafts, short-dashed curves and o: environmental air. (a) Area fraction of plumes, (b) number of plumes per unit length, averaged over both directions, (c) mean diameter of plumes.

Fig. 6. Comparison as in Fig. 5. (a) vertical velocity, (b) deviation in virtual potential temperature from the horizontally averaged profile, (c) deviation in wind speed in x-direction from average profile.

Fig. 7. Comparison as in Fig. 5. (a) vertical buoyancy flux, (b) momentum flux, normalized by the surface fluxes.

Fig. 8. Computed values from LES for case CTBL (curves) with measured data (symbols) from Nicholls (1989). (a) diameter of downdrafts in x (full curve) and y directions (dashed), (b) number of downdrafts per unit length in both directions as before, (c) area fraction of downdrafts.

Fig. 9. Properties of updrafts (u), downdrafts (d) and environmental air (e) in a CTBL for wq-plumes. (a) diameter in x direction, (b) number of plumes per unit length in x and y directions and its average, (c) area fractions.

Fig. 10. Differences between mean values in updrafts and downdrafts for wq-plumes in a CTBL as computed (curves) and measured by Penc and Albrecht (1987) (circles from flight 4, squares from flight 5). The measured data refer to the upper normalized ordinate. (a) differences in total (Δq) and liquid water content (Δq_ℓ), (b) differences in liquid water potential temperature ($\Delta\theta_\ell$) and virtual potential temperature ($\Delta\theta_v$).

Fig. 11. Normalized fluxes in the the CBL. (a) heat flux, (b) momentum flux, (c) vertical velocity variance. Full curves: total flux, dashed curves: top-hat profile approximation for w-plumes, dash-dotted curves: same for T-plumes.

Fig. 12. Fluxes in the CTBL. (a) heat flux, (b) latent heat flux, (c) momentum flux, (d) buoyancy flux, (e) liquid water flux (f) normalized vertical velocity variance. Full curves: total flux, long-dashed curves: top-hat profile approximation for w-plumes, dash-dotted curves: same for q-plumes, short-dashed curves: same for wq-plumes.

Fig. 13. Coefficients a, b, and flux velocity ω^*/w_{*D}, as defined in Eqs. (1, 3, 4), for w-plumes with zero threshold values. Left: CBL, right: CTBL. The various curves result from different values of the transported quantity f. Solid: θ (or θ_ℓ for CTBL), long dashed: u, short dashed: w, dash-dotted: q.

Fig. 14. Flux velocity ω^{**}/w_*, as defined in Eq. (2), for w-plumes with non-zero threshold values as defined by Greenhut and Khalsa (1987), for the CBL. The circles indicate data from these authors. Solid: $f = \theta$, long dashed: u, short dashed: w.

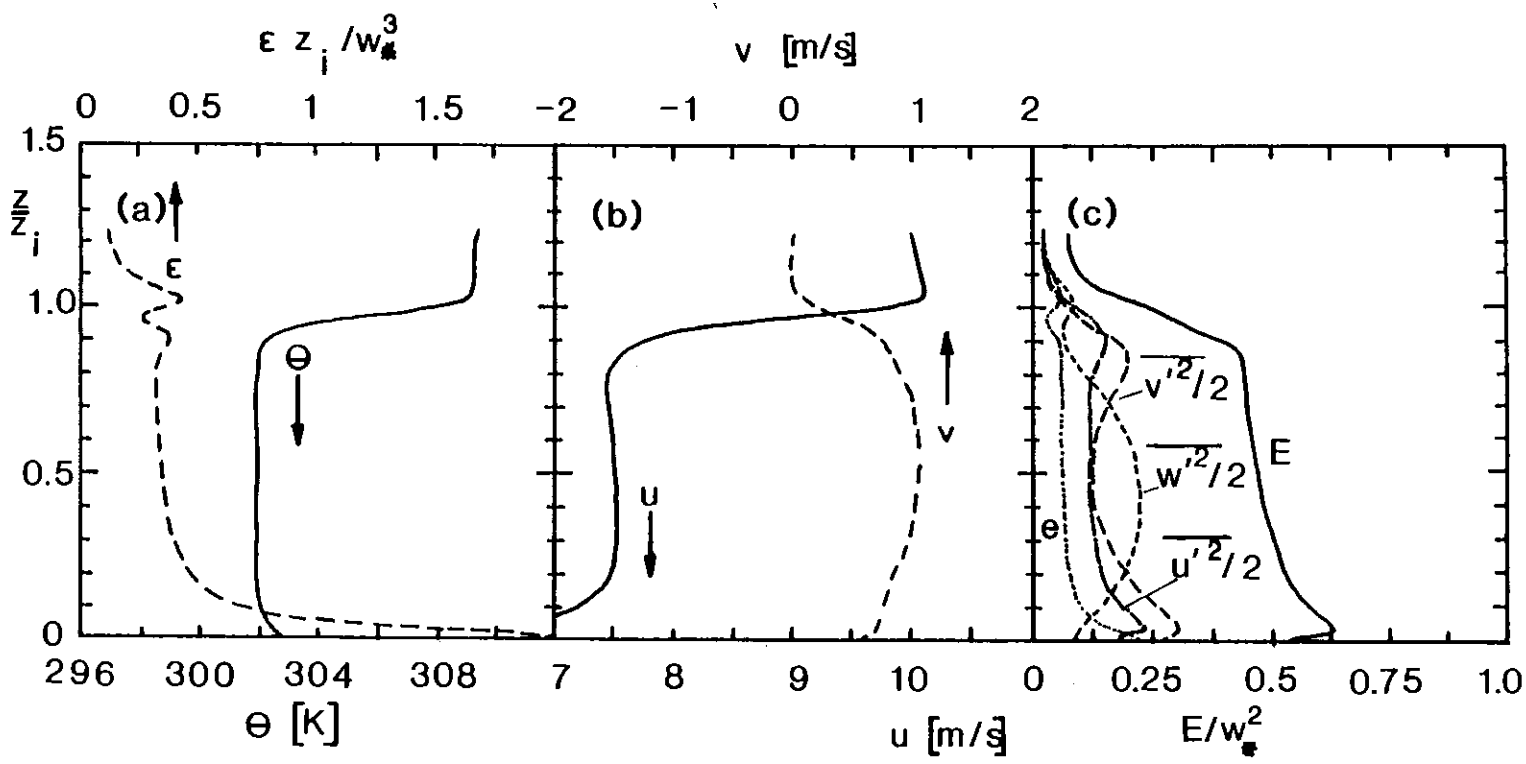

Fig. 1. Mean profiles in the CBL. (a) potential temperature and normalized dissipation rate, (b) horizontal wind components, (c) turbulent kinetic energy of all scales *E*, subgrid-scale kinetic energy *e*, and energy of the three velocity components.

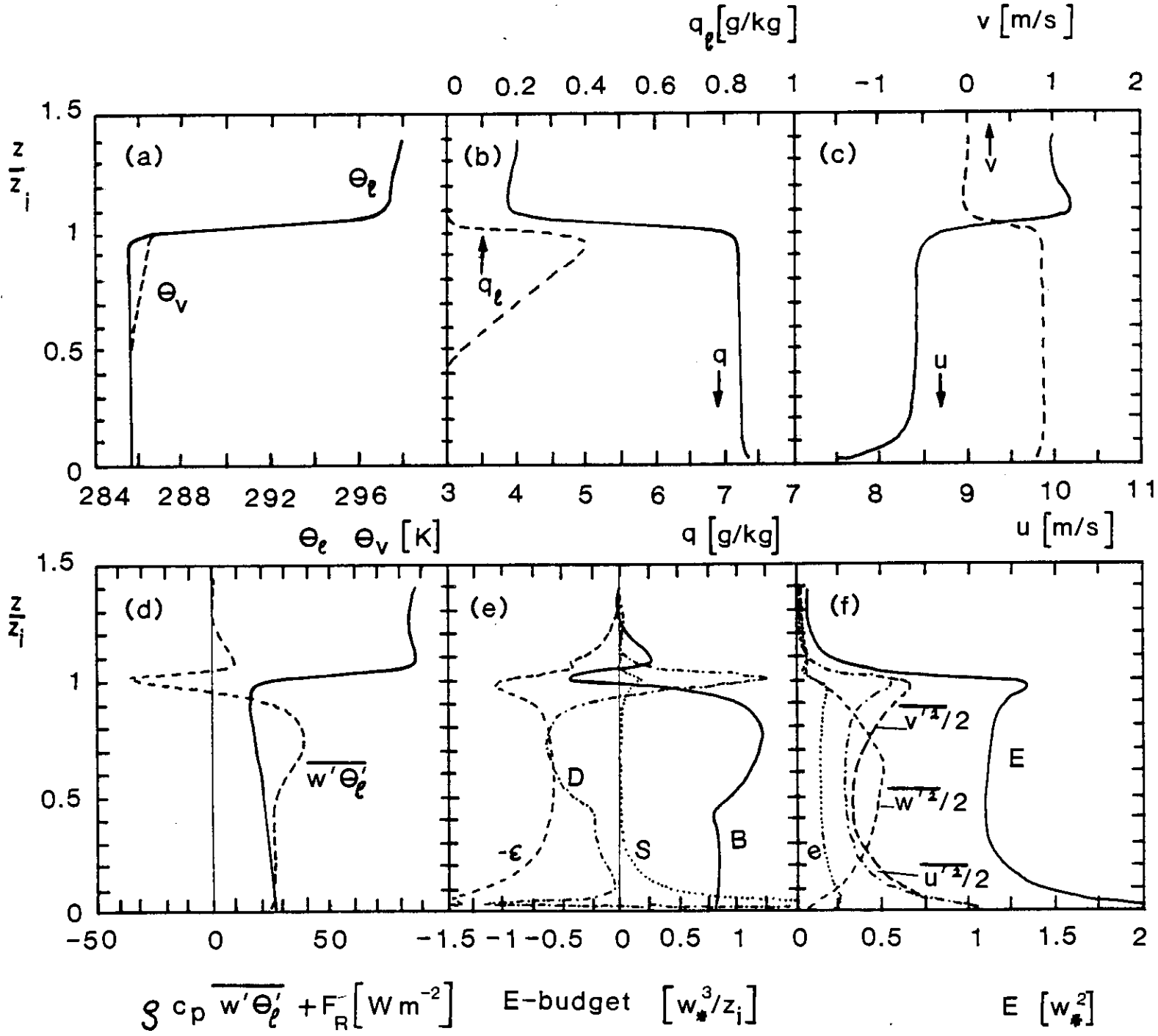

Fig. 2. Mean profiles in the CTBL. (a) liquid water potential temperature (full curve) and virtual potential temperature (dashed), (b) total and liquid water content, (c) wind components, (d) sum of liquid water static energy and longwave radiation fluxes (full curve) and liquid water static energy flux alone (dashed), (e) budget of kinetic energy due to buoyancy B, shear S, dissipation ε, and diffusion D, (f) total kinetic turbulence energy E, SGS energy e, and variance components.

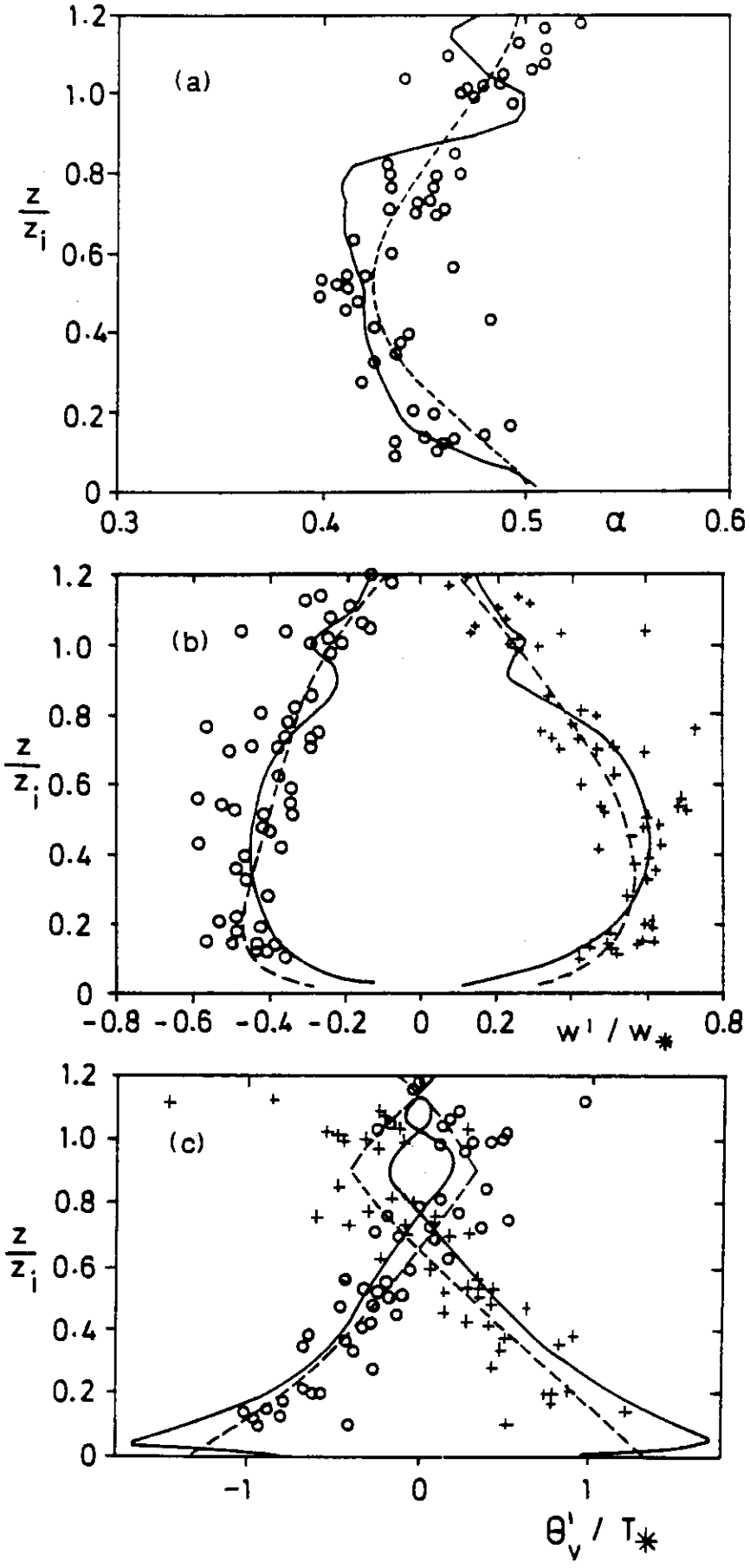

Fig. 3. Comparison of w-plume mean values computed from LES for case CBL (full curves) with measured data (symbols) and corresponding interpolations (dashed curves) from Young (1988). (a) Area fraction of updrafts, (b) updraft and downdraft velocities, (c) potential temperature deviations in updrafts and downdrafts relative to the horizontally averaged potential temperature.

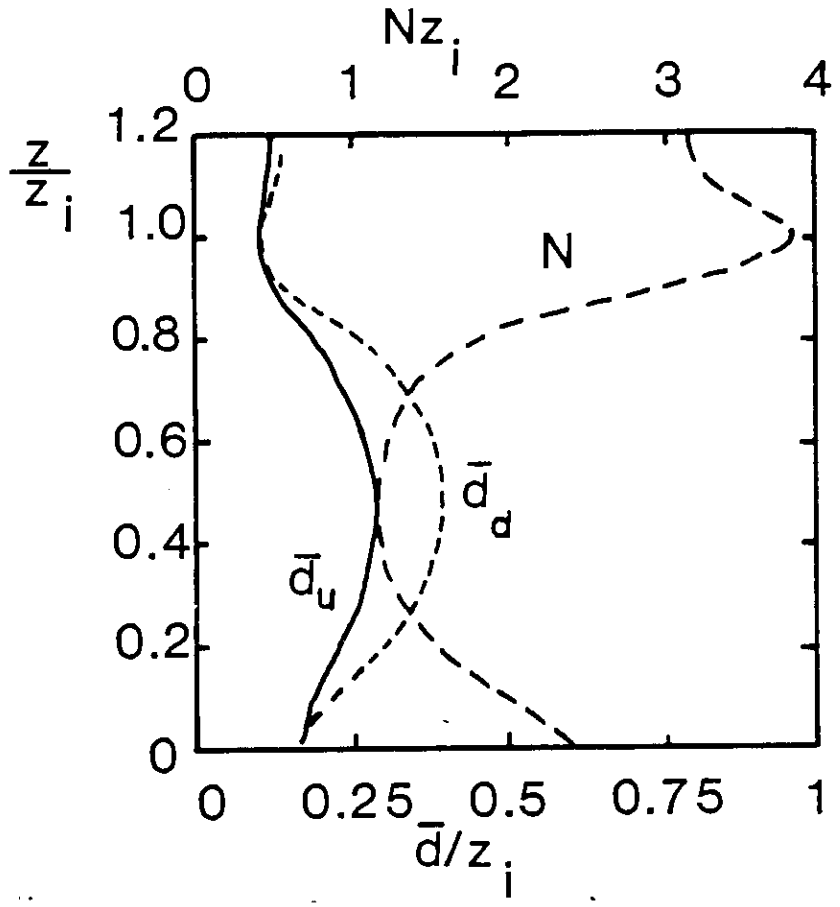

Fig. 4. Mean diameters $\bar{d}$ of updrafts and downdrafts and number N of updrafts per unit length (averaged over both horizontal directions) for case CBL, w-plumes.

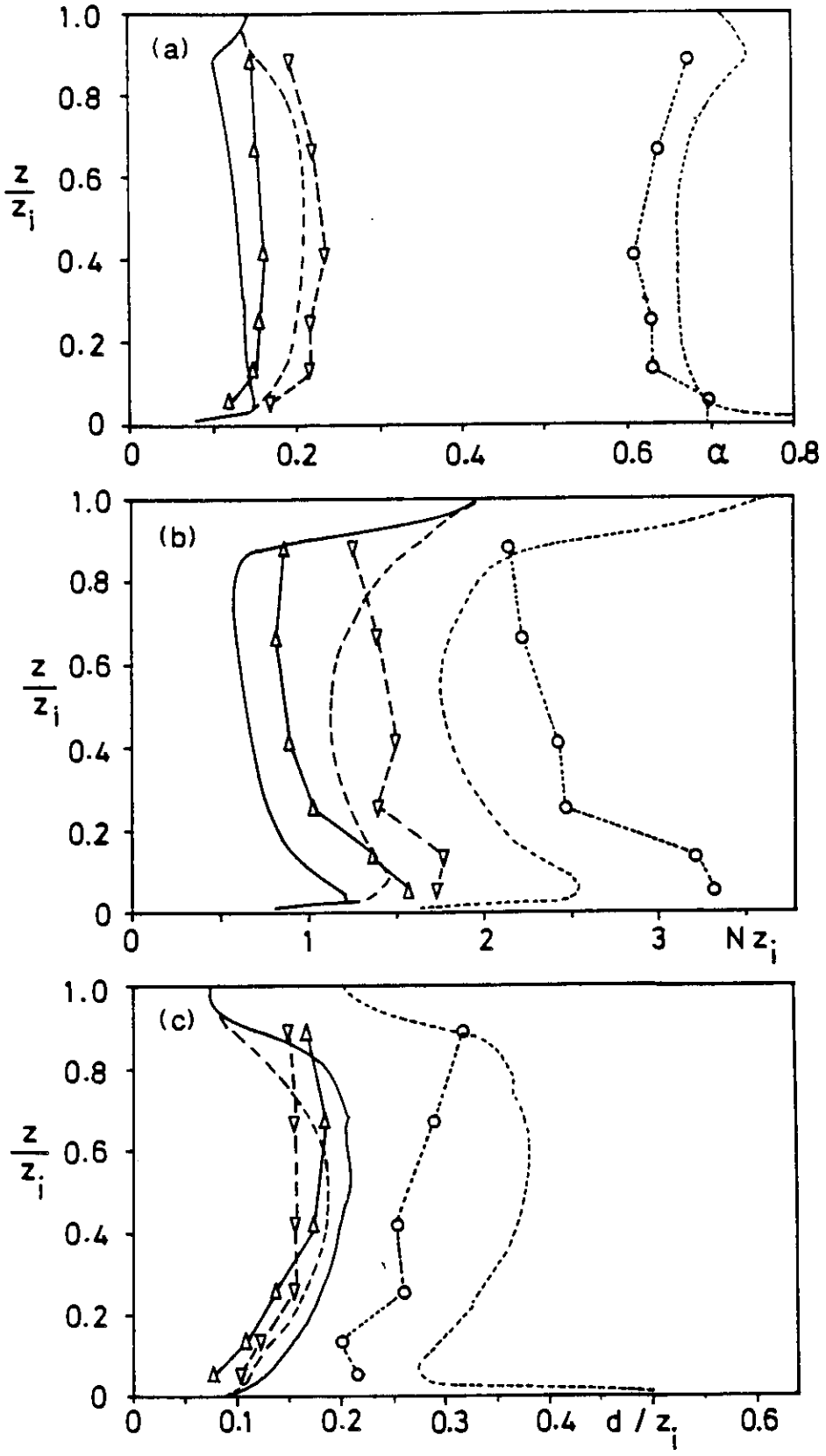

Fig. 5. Comparison of plume mean values computed for case CBL (curves without symbols) with measured data (curves with symbols) from Greenhut and Khalsa (1987). Full curves and Δ: updrafts, dashed curves and ∇: downdrafts, short-dashed curves and o: environmental air. (a) Area fraction of plumes, (b) number of plumes per unit length, averaged over both directions, (c) mean diameter of plumes.

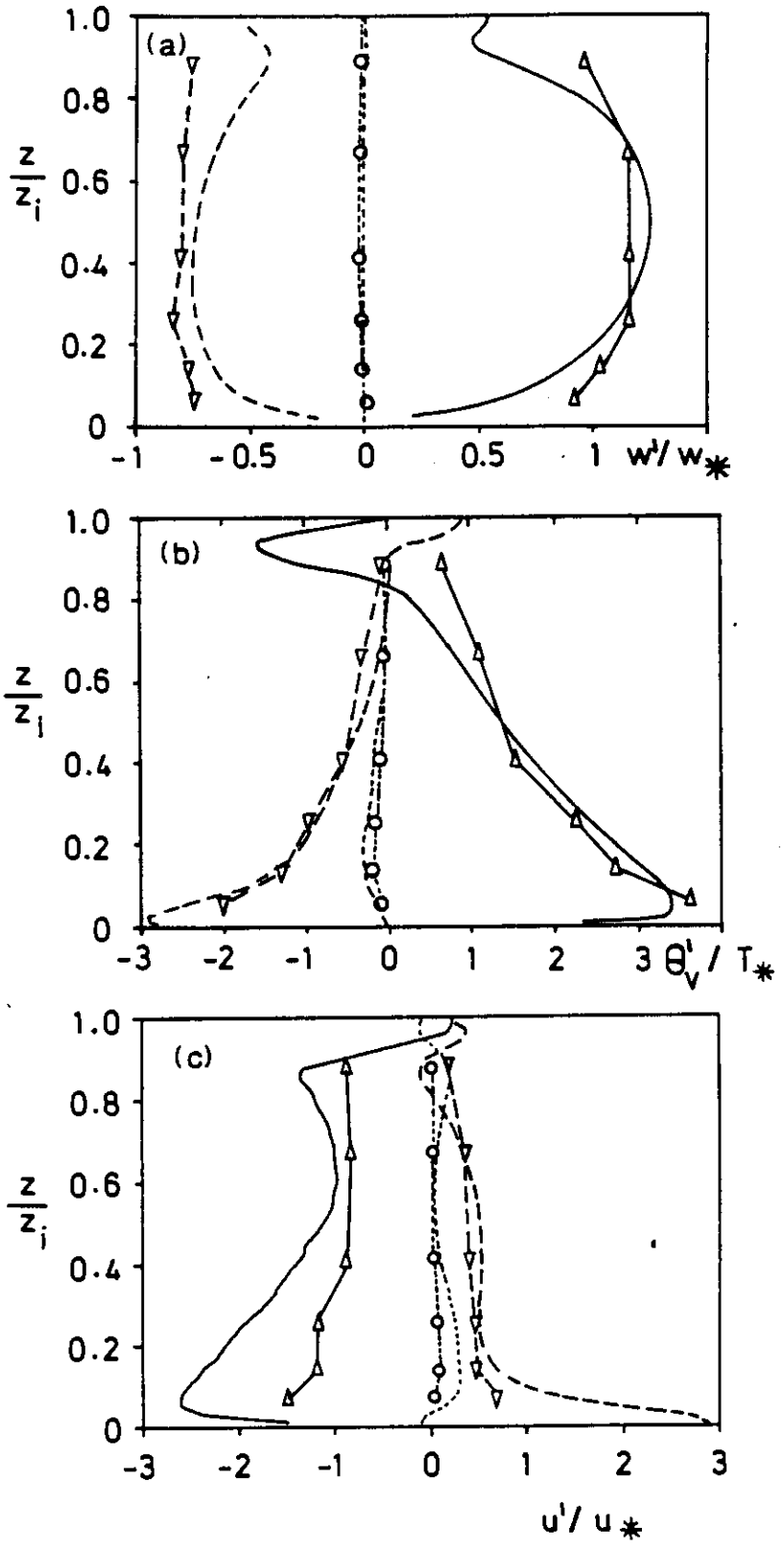

Fig. 6. Comparison as in Fig. 5. (a) vertical velocity, (b) deviation in virtual potential temperature from the horizontally averaged profile, (c) deviation in wind speed in *x*-direction from average profile.

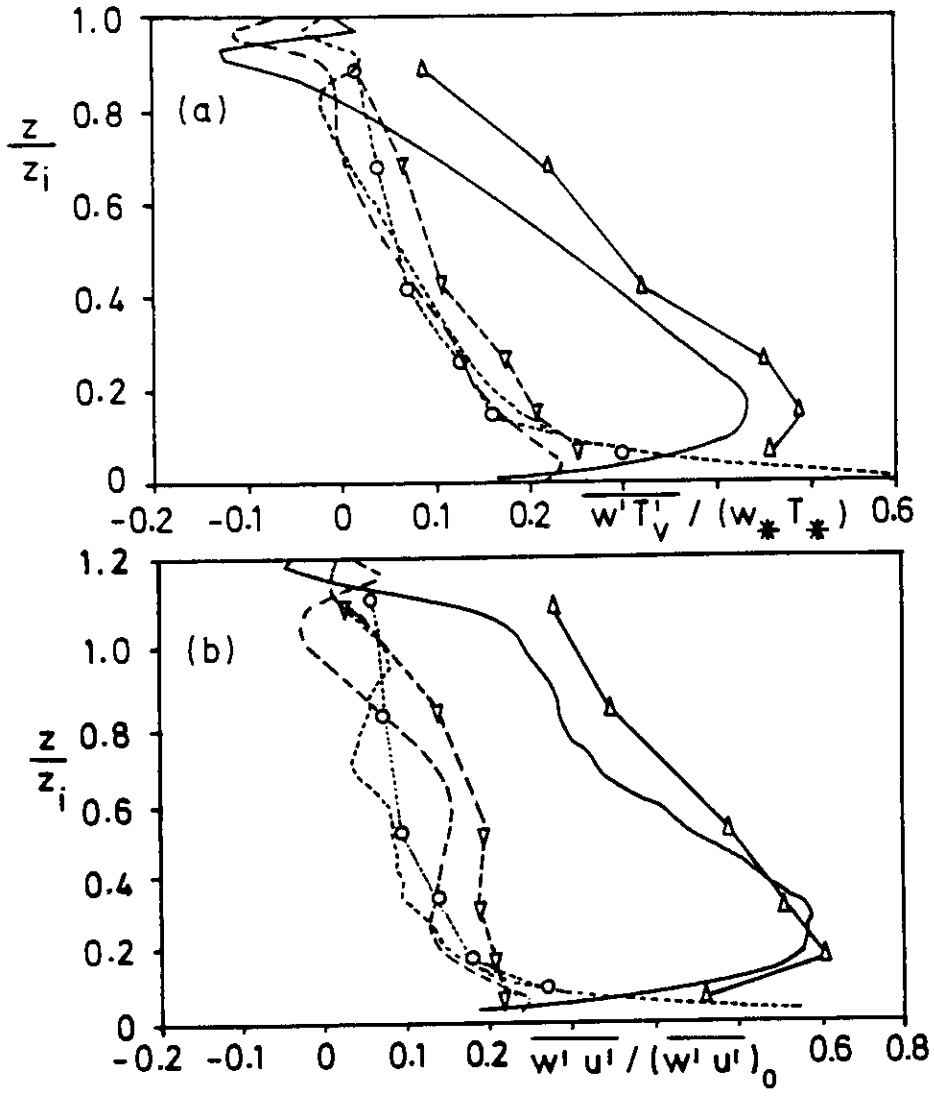

Fig. 7. Comparison as in Fig. 5. (a) vertical buoyancy flux, (b) momentum flux, normalized by the surface fluxes.

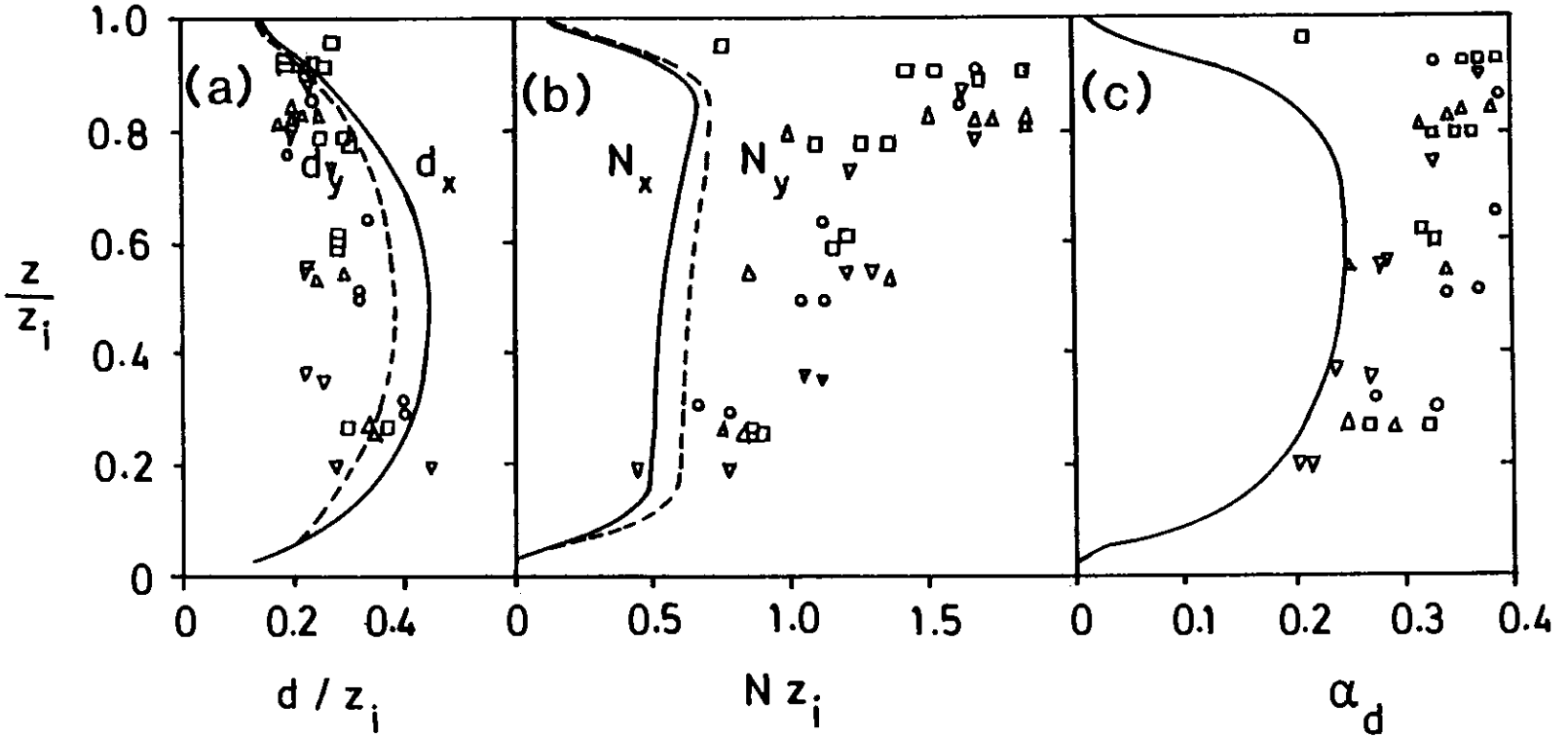

Fig. 8. Computed values from LES for case CTBL (curves) with measured data (symbols) from Nicholls (1989). (a) diameter of downdrafts in x (full curve) and y directions (dashed), (b) number of downdrafts per unit length in both directions as before, (c) area fraction of downdrafts.

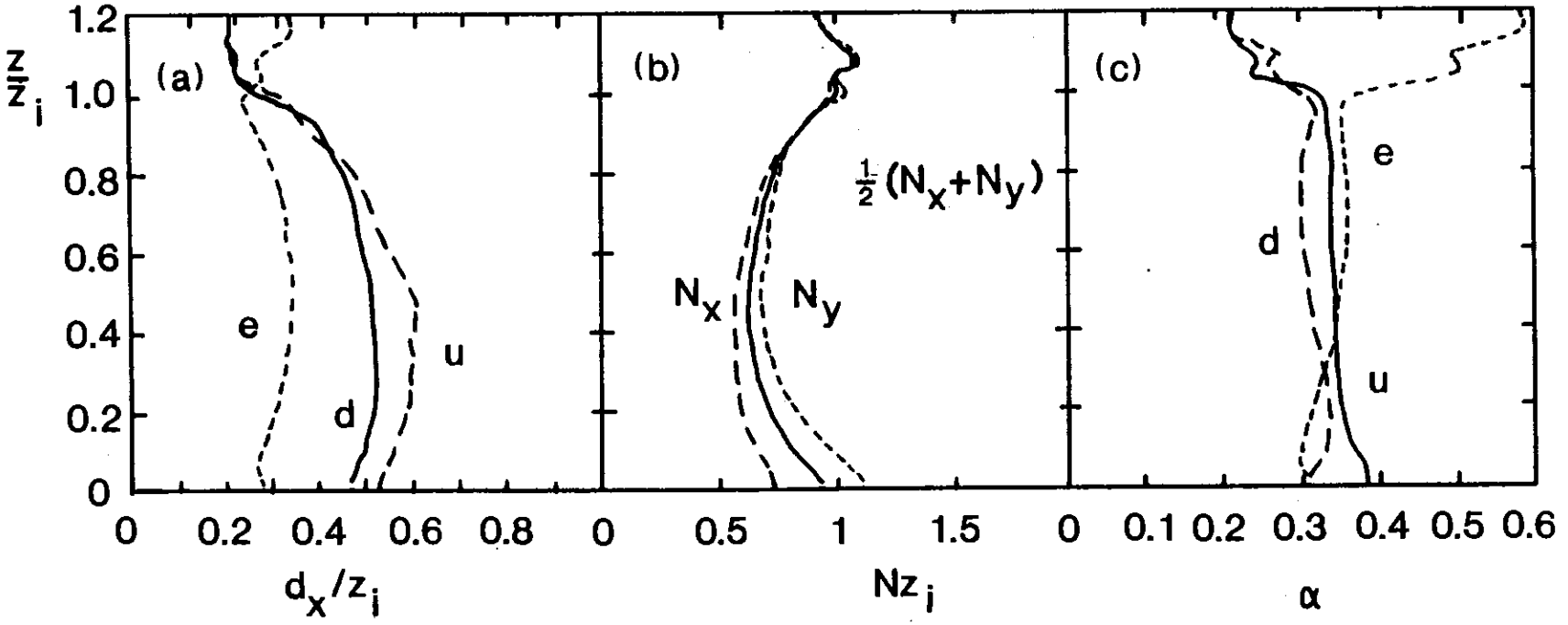

Fig. 9. Properties of updrafts (u), downdrafts (d) and environmental air (e) in a CTBL for wq-plumes. (a) diameter in x direction, (b) number of plumes per unit length in x and y directions and its average, (c) area fractions.

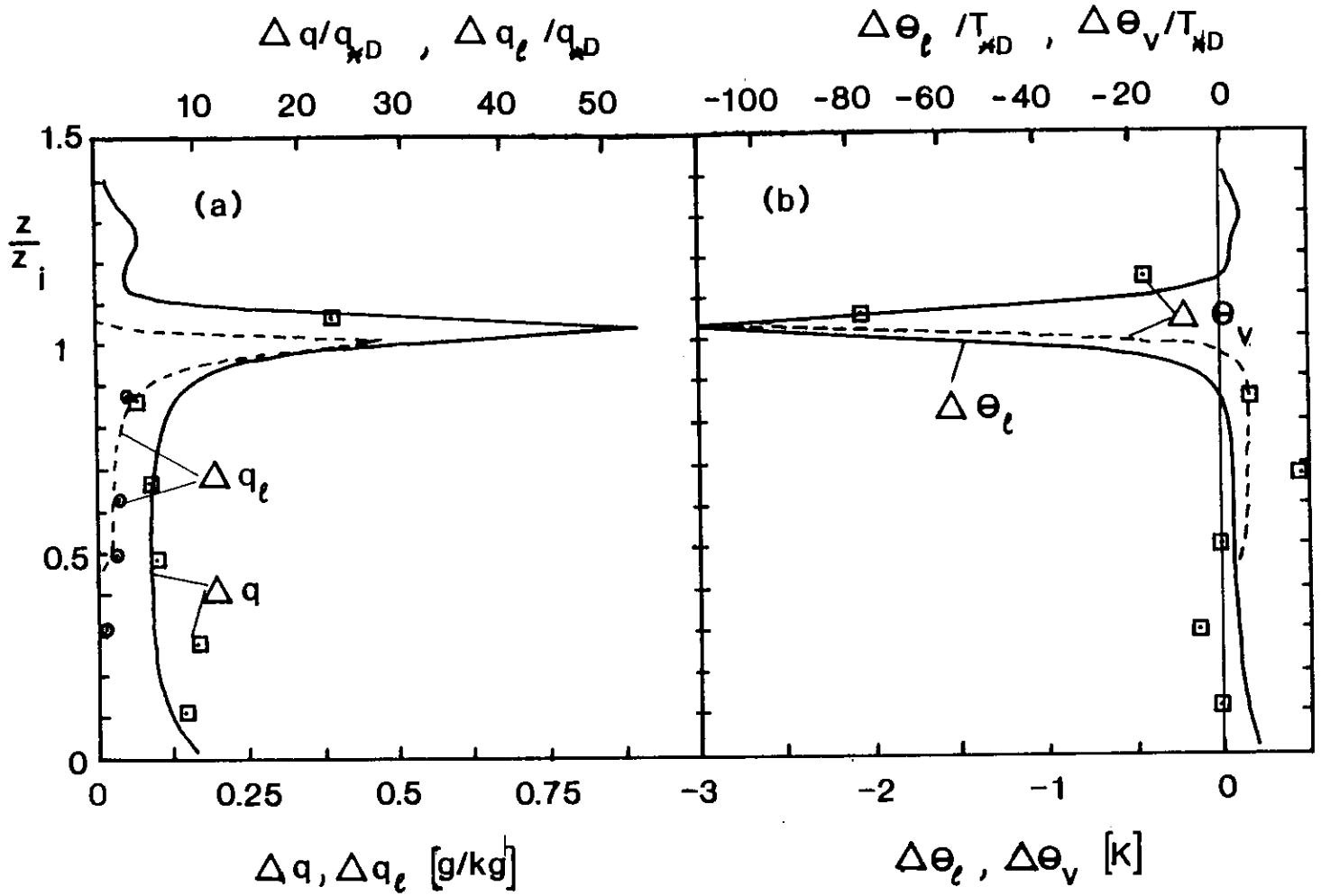

Fig. 10. Differences between mean values in updrafts and downdrafts for wq-plumes in a CTBL as computed (curves) and measured by Penc and Albrecht (1987) (circles from flight 4, squares from flight 5). The measured data refer to the upper normalized ordinate. (a) differences in total (Δq) and liquid water content (Δq_ℓ), (b) differences in liquid water potential temperature ($\Delta\theta_\ell$) and virtual potential temperature ($\Delta\theta_v$).

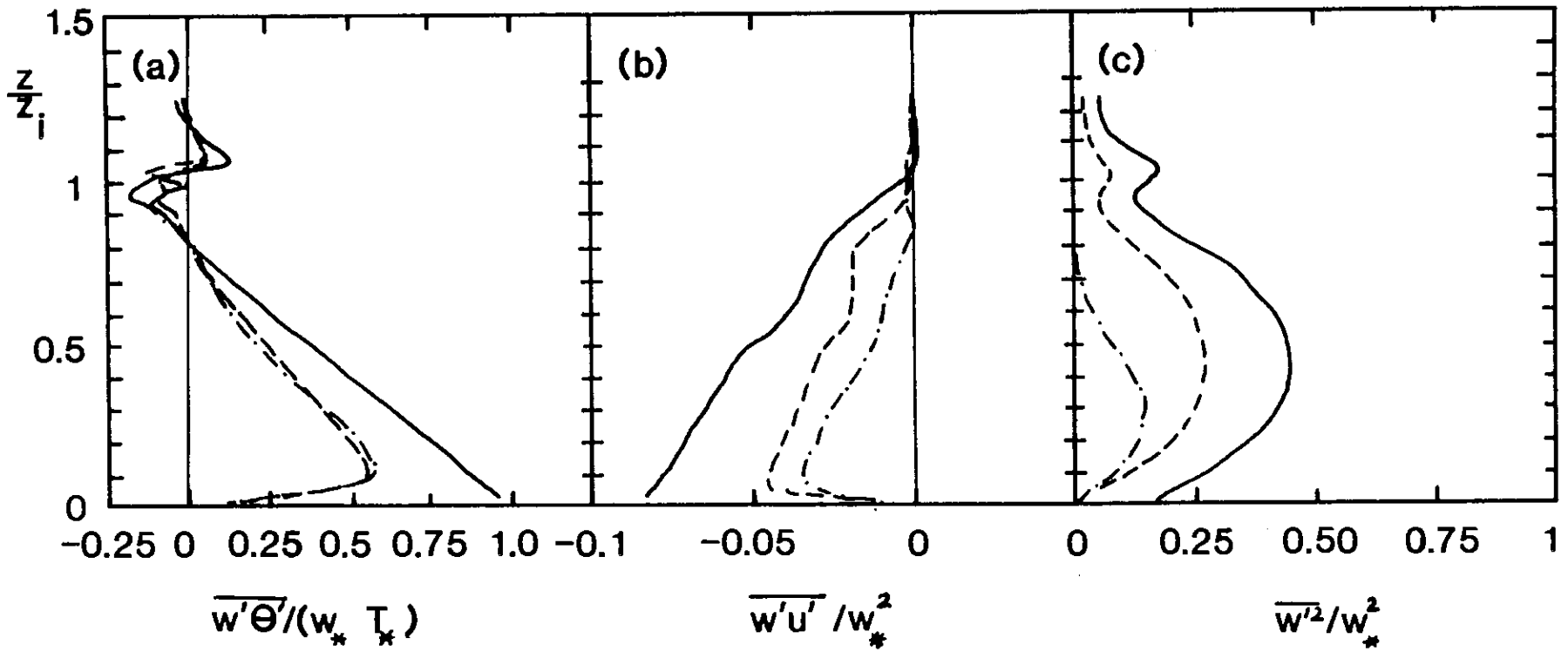

Fig. 11. Normalized fluxes in the the CBL. (a) heat flux, (b) momentum flux, (c) vertical velocity variance. Full curves: total flux, dashed curves: top-hat profile approximation for w-plumes, dash-dotted curves: same for T-plumes.

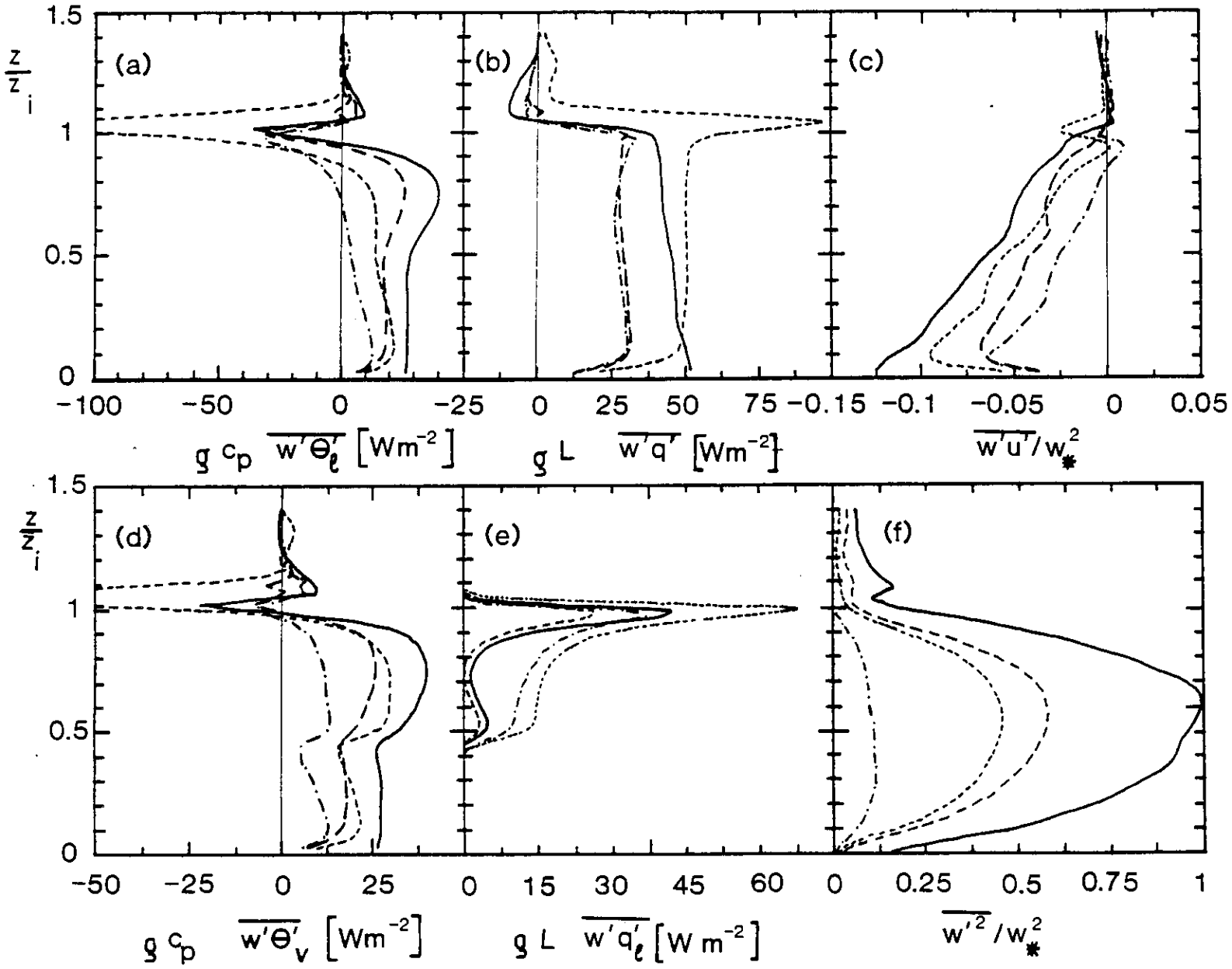

Fig. 12. Fluxes in the CTBL. (a) heat flux, (b) latent heat flux, (c) momentum flux, (d) buoyancy flux, (e) liquid water flux (f) normalized vertical velocity variance. Full curves: total flux, long-dashed curves: top-hat profile approximation for w-plumes, dash-dotted curves: same for q-plumes, short-dashed curves: same for wq-plumes.

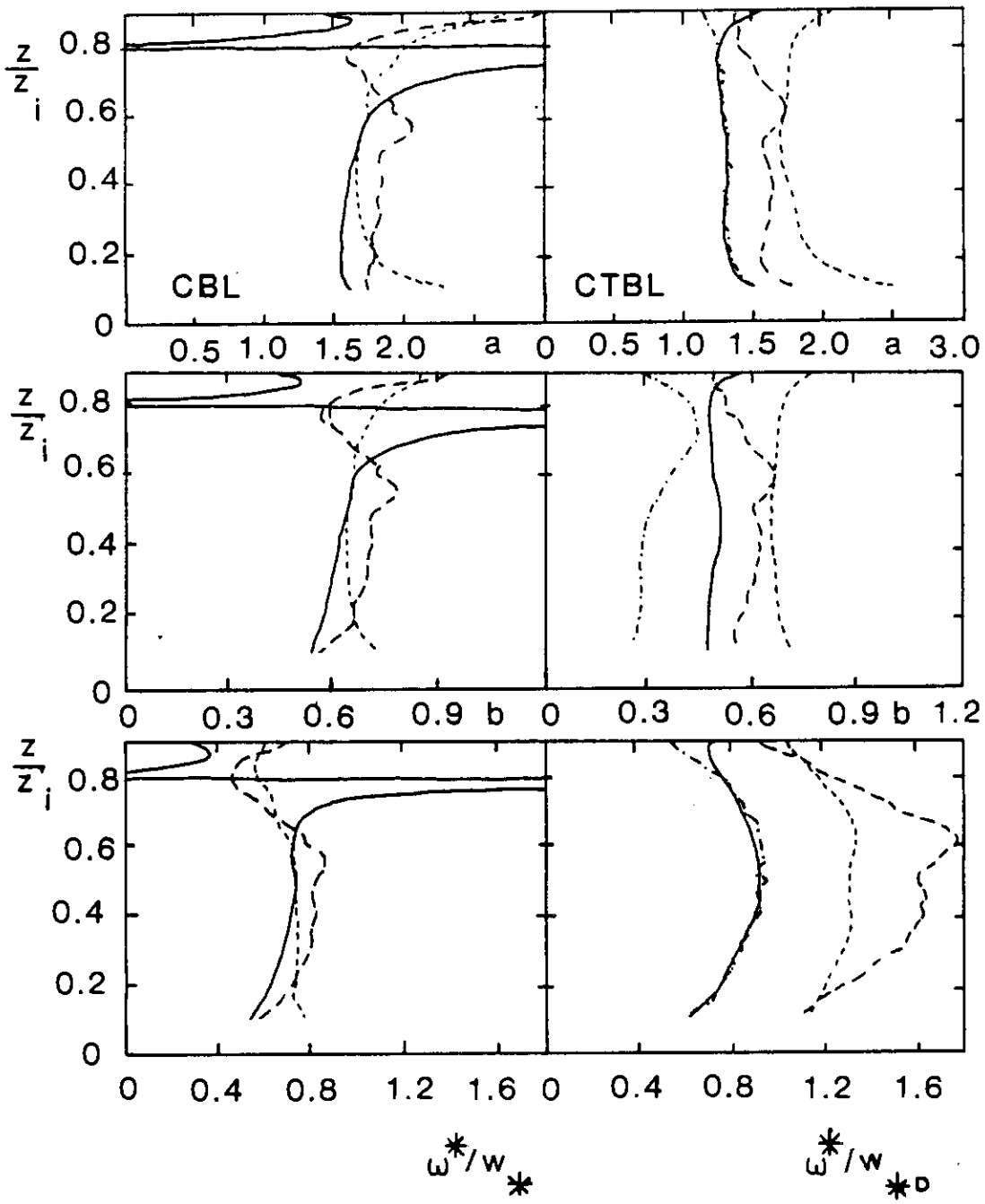

Fig. 13. Coefficients *a*, *b*, and flux velocity ω^*/w_{*D}, as defined in Eqs. (1, 3, 4), for w-plumes with zero threshold values. Left: CBL, right: CTBL. The various curves result from different values of the transported quantity *f*. Solid: θ (or θ_ℓ for CTBL), long dashed: *u*, short dashed: *w*, dash-dotted: *q*.

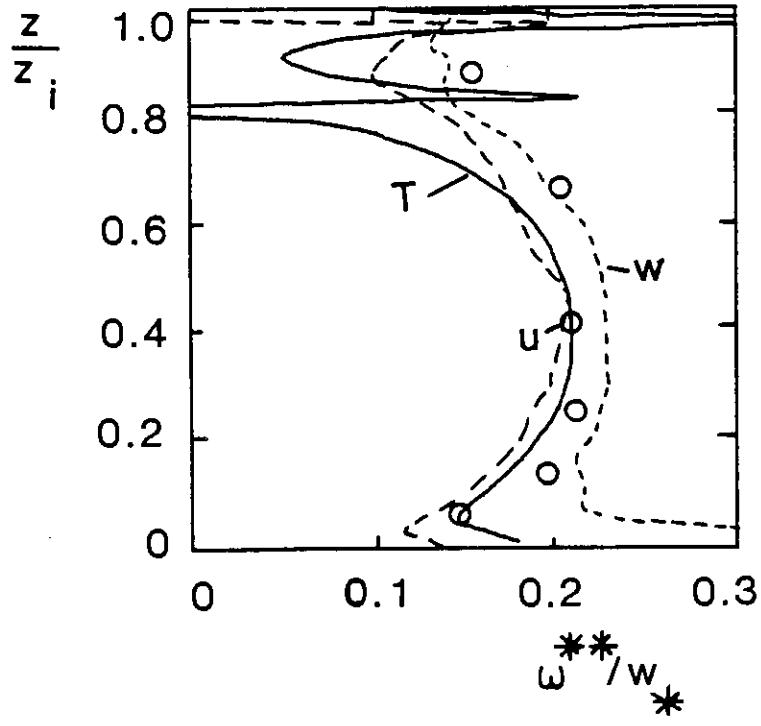

Fig. 14. Flux velocity ω^{**}/w_*, as defined in Eq. (2), for w-plumes with non-zero threshold values as defined by Greenhut and Khalsa (1987), for the CBL. The circles indicate data from these authors. Solid: $f = \theta$, long dashed: u, short dashed: w.